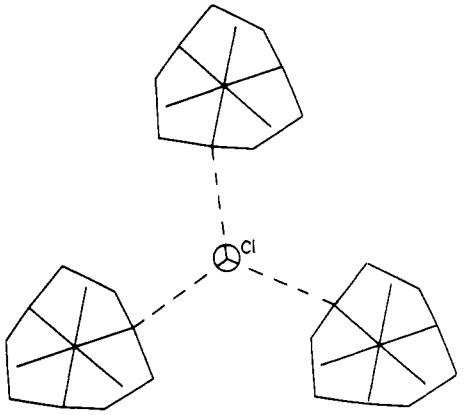

Figure 2. Packing diagram of one layer of $[LReO_3]^+$ cations and a chloride ion (viewed down the *c* axis) emphasizing the N-H···Cl hydrogen bonding (broken lines).

Description of the Crystal Structure of $[LReO_3]Cl$. Crystals of $[LReO_3]Cl$ consist of $[LReO_3]^+$ cations and uncoordinated chloride ions. Figure 1 shows a perspective view of the complex cation and the atomic labeling scheme. The cation possesses crystallographically imposed C_3 symmetry. The rhenium centers are in a highly distorted octahedral environment of three facially coordinated nitrogen atoms of the macrocyclic ligand and three facially coordinated oxygen atoms.

The Re-O bond distance of 1.756 (5) Å is rather short, indicating considerable double-bond character. Interestingly, in $Re_2O_7(OH_2)_2$, which has a dimeric molecular structure containing one distorted tetrahedral ReO_4^- and an octahedral $ReO_3(OH_2)_2^+$ unit connected by a linear oxo bridge,[18] the terminal Re=O bond distance in the octahedral part is found to be 1.75 Å. The same distance has been observed for $(\eta^5\text{-}Me_5C_5)ReO_3$[9] and for $Re_2O_7(C_5H_5N)_3$.[21]

The Re-N bond length of 2.197 (5) Å is quite long, which indicates a pronounced trans influence of the terminal oxo groups. Re-N bonds in rhenium(V) oxo complexes range from 2.11 to 2.16 Å, e.g. in $[ReO_2(4\text{-Mepy})_4]ReO_4$ and related complexes.[19]

The N-Re-N bond angles of nitrogen atoms in cis positions with respect to each other are considerably smaller (76.5 (3)°) than the ideal octahedral angle of 90°. This is mainly due to the steric constraints of the cyclononane ring and the rather long Re-N bond lengths. On the other hand, the O-Re-O bond angles of oxygen atoms in cis positions are obtuse (102.7 (4)°). This reflects the known tendency of oxo complexes of transition metals in very high oxidation states (d^0 electronic configuration) with short M-O distances to maximize the otherwise short approaches of nonbonded oxygen atoms.

It is of interest to compare the present structure with that of $(dien)MoO_3$.[20] The geometry of the MoO_3N_3 core is remarkably similar to that found in $[LReO_3]^+$ (N-Mo-N = 75°, O-Mo-O = 106°; Mo=O = 1.736 Å, Mo-N = 2.324 Å). The structure of $[LReO_3]Cl$ consists of hexagonal-close-packed layers containing both the $[LReO_3]^+$ cations and chloride ions, stacked along the *c* axis. Each $[LReO_3]^+$ ion has a packing relationship with three chloride ions that includes hydrogen bonding between all three amine nitrogen atoms of the coordinated cyclic ligand. Each chloride ion is connected via N-H···Cl hydrogen bonds to three $[LReO_3]^+$ cations (Figure 2). The N···Cl distance is 3.167 (6) Å. The oxygen atoms of $[LReO_3]^+$ are not involved in this hydrogen-bonding scheme.

Acknowledgment. We thank the Fonds der Chemischen Industrie for financial support and Degussa (Hanau) for a generous loan of rhenium metal.

Registry No. $[LRe(CO)_3]Br$, 101566-53-4; $Re(CO)_5Br$, 14220-21-4; $[LRe(NO)(CO)_2](BF_4)_2$, 101566-55-6; $[LReO_3]Cl$, 101566-56-7; $[LReO_3]ReO_4$, 101566-58-9.

Supplementary Material Available: Tables of anisotropic thermal parameters, calculated positional parameters of hydrogen atoms, and intraligand bond distances and angles (2 pages). Ordering information is given on any current masthead page. According to policy instituted Jan 1, 1986, the tables of calculated and observed structure factors (7 pages) are being retained in the editorial office for a period of 1 year following the appearance of this work in print. Inquiries for copies of these materials should be directed to the Editor.

(18) Beyer, H.; Glemser, D.; Krebs, B. *Angew. Chem.* **1968**, *80*, 286.
(19) Johnson, J. W.; Brody, J. F.; Ansell, G. B.; Zentz, S. *Inorg. Chem.* **1984**, *23*, 2415.
(20) Cotton, F. A.; Elder, R. C. *Inorg. Chem.* **1964**, *3*, 397.
(21) Johnson, J. W.; Brody, J. F.; Ansell, G. B.; Zentz, S. *Acta Crystallogr., Sect. C: Cryst. Struct. Commun.* **1984**, *C40*, 2024.

Contribution from the Inorganic Chemistry Laboratory, University of Oxford, Oxford OX1 3QR, U.K.

Theoretical Analysis of the Bonding in Octahedral Transition-Metal Clusters Containing π-Acceptor and π-Donor Bridging Ligands and Their Nido and Arachno Derivatives

Roy L. Johnston and D. Michael P. Mingos*

Received April 1, 1985

The bonding in octahedral clusters with face- and edge-bridging ligands has been studied by semiempirical molecular orbital calculations and interpreted within the framework of Stone's tensor surface harmonic theory. The function of π-acceptor and π-donor ligands in stabilizing the metal-metal bonding in clusters is discussed, and the role of the metal orbitals with δ symmetry in influencing the observed electron counts is stressed. Calculations on nido and arachno structures based on $[Mo_6Cl_{18}]^{2+}$, with edge-bridging ligands, have suggested that they behave analogously to metal carbonyl clusters, and the number of skeletal bonding molecular orbitals remains constant in the closo, nido, and arachno series. In contrast, the closo, nido, and arachno structures derived from $[Mo_6Cl_{14}]^{2-}$ with face-bridging ligands have $3n - 6$ skeletal bonding molecular orbitals where n is the number of metal atoms. The differences in electron counts in clusters with edge- and face-bridging ligands can be rationalized in terms of the complementary nature of the interactions between the metal d^6 and the ligand orbitals in the two cases.

Introduction

During the last 10 years the growth of transition-metal carbonyl cluster chemistry[1] has been assisted by the development of a simple electron-counting rules[2] that relate the total number of valence electrons to topological features of the metal polyhedra. These electron-counting rules have been underpinned theoretically by calculations on individual cluster molecules,[3] the development of

(1) *Transition Metal Clusters*; Johnson, B. F. G., Ed.; Wiley: 1980, and references therein.

(2) (a) Wade, K. *Adv. Inorg. Chem. Radiochem.* **1976**, *18*, 1. (b) Mingos, D. M. P. *Nature (London), Phys. Sci.* **1972**, *236*, 99. (c) Mingos, D. M. P. *Acc. Chem. Res.* **1984**, *17*, 311.

0020-1669/86/1325-1661$01.50/0

the *isolobal* approach,[4] and most recently, the elegant tensor surface harmonic mode of analysis introduced by Stone.[5]

These electron-counting rules are not directly transferable to clusters formed by the early transition metals with bridging π-donor ligands such as Cl, Br, S, and OR (R = alkyl group),[6] e.g. $[M_6Cl_8L_6]^{4+}$ (I) (M = Mo or W) and $[M_6Cl_{12}L_6]^{2+}$ (II) (M = Nb or Ta). The former cluster has eight ligands arranged in a

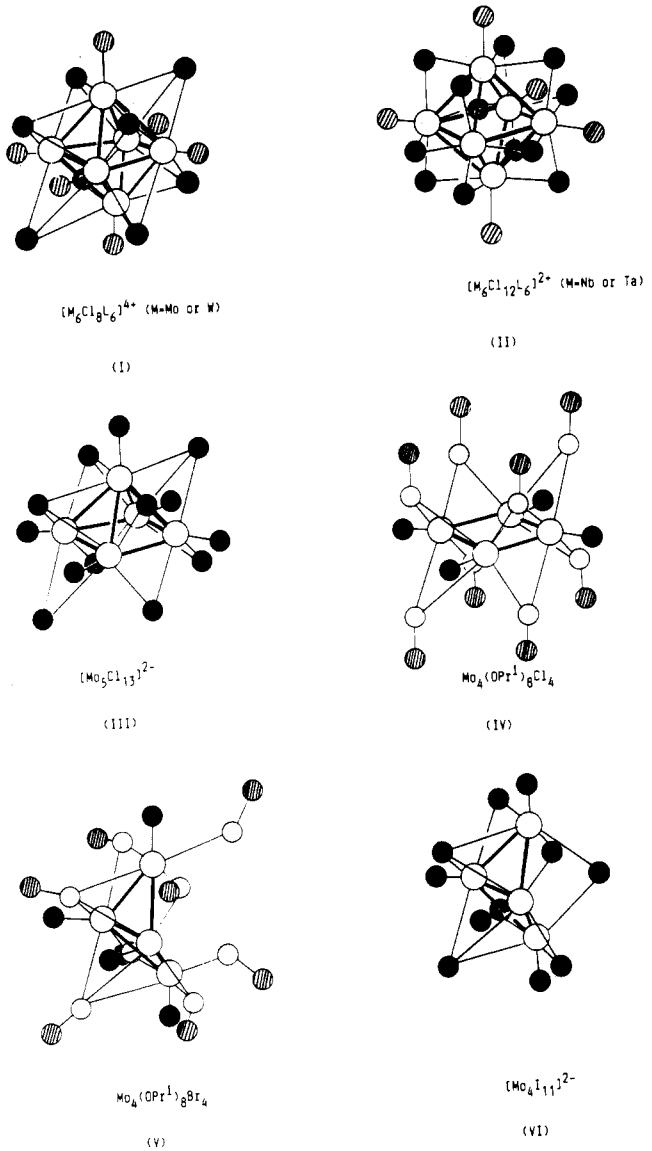

cubic manner and bridging the faces of the octahedral cluster. In structures such as $[MoCl_2]_n$ the terminal ligands also act as bridging ligands between the cluster units,[7] but discrete $[Mo_6Cl_{14}]^{2-}$ ions are known for example in $(NH_4)_2[Mo_6Cl_{14}]\cdot H_2O$.[8] The second type of cluster has 12 ligands arranged in a cuboctahedral fashion and functioning as edge-bridging ligands to the octahedral metal cluster. The remaining six terminal ligands may act as bridging ligands between clusters, e.g. $[Nb_6Cl_{12}]Cl_2$,[9] but discrete $[M_6Cl_{18}]^{4-}$ ions have also been characterized, as in $K_4[Nb_6Cl_{18}]$.[10]

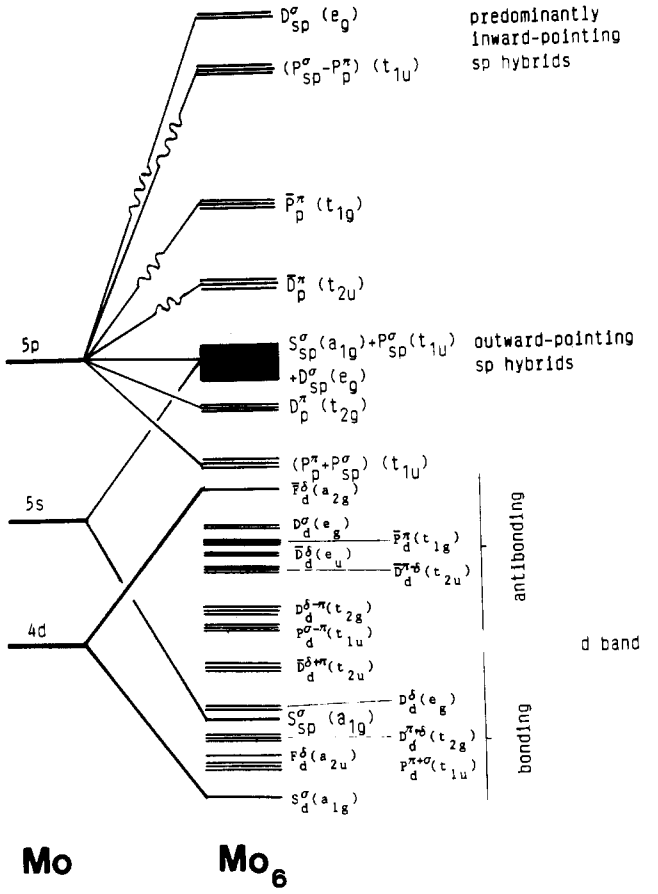

Figure 1. Schematic molecular orbital diagram for a "naked" Mo_6 octahedral cluster.

The bonding in these octahedral clusters may be adequately described in terms of localized-bonding schemes.[11] The face-bridged cluster possesses 12 skeletal electron pairs (sep's) corresponding to the formation of localized two-center two-electron bonds along the edges of the cluster. In contrast, the edge-bridged cluster possesses eight sep's corresponding to localized three-center two-electron bonds on the faces of the octahedron. Therefore, there exists a complementary relationship between the positions of the bridging ligands and the disposition of the localized metal–metal bonds. Such localized-bonding schemes are not applicable to metal–carbonyl octahedral clusters.

The total polyhedral electron counts for the face- and edge-bridged octahedral π-donor clusters are 84 and 76, respectively.[12] These differ from the 86-electron ($14n + 2$) count generally associated with metal carbonyl clusters.[12] This obvious difference in electron counts for π-donor and π-acceptor clusters provided the initial stimulus for this theoretical analysis. Furthermore, the two classes of clusters show interesting electronic differences when metal atoms are removed from the octahedral clusters. Metal carbonyl clusters may be classified by the closo, nido, and arachno scheme originally developed for boranes. This scheme forges a

(3) (a) Lauher, J. W. *J. Am. Chem. Soc.* **1978**, *100*, 5305. (b) Manning, M. C.; Trogler, W. C. *Coord. Chem. Rev.* **1981**, *38*, 89 and references therein. (c) Cheskey, P. T.; Hall, M. B. *Inorg. Chem.* **1981**, *20*, 4419. Sherwood, D. E.; Hall, M. B. *Inorg. Chem.* **1982**, *21*, 3458. Sherwood, D. E.; Hall, M. B. *Organometallics* **1982**, *1*, 1519. (d) Johnston, R. L.; Mingos, D. M. P. *J. Organomet. Chem.* **1985**, *280*, 419.

(4) (a) Elian, M.; Chen, M. M. L.; Mingos, D. M. P.; Hoffmann, R. *Inorg. Chem.* **1976**, *15*, 1148. Hoffmann, R. *Angew. Chem., Int. Ed. Engl.* **1982**, *21*, 711.

(5) (a) Stone, A. J. *Mol. Phys.* **1980**, *41*, 1339. (b) Stone, A. J. *Inorg. Chem.* **1981**, *20*, 563. (c) Stone, A. J.; Alderton, M. J. *Inorg. Chem.* **1982**, *21*, 2297. (d) Stone, A. J. *Polyhedron* **1984**, *3*, 1299.

(6) (a) McCarley, R. E. *Philos. Trans. R. Soc. London A* **1982**, *308*, 141 and references therein. (b) Corbett, J. D. *Acc. Chem. Res.* **1981**, *14*, 239. (c) Chevrel, R.; Sergent, M.; Prigent, J. *J. Solid State Chem.* **1971**, *3*, 515. (d) Chevrel, R.; Gougeon, P.; Potel, M.; Sergent, M. *J. Solid State Chem.* **1985**, *57*, 25. (e) Simon, A. *Angew. Chem., Int. Ed. Engl.* **1981**, *20*, 1.

(7) Schafer, H.; Schnering, H. G. *Angew. Chem.* **1964**, *76*, 833.

(8) Vaughan, P. A. *Proc. Natl. Acad. Sci. U. S. A.* **1950**, *36*, 461.

(9) Simon, A.; Schnering, H. G.; Wohrle, H.; Schafer, H. *Z. Anorg. Allg. Chem.* **1965**, *339*, 155.

(10) Simon, A.; Schnering, H. G.; Schafer, H. *Z. Anorg. Allg. Chem.* **1968**, *361*, 235.

(11) Kettle, S. F. A. *Theor. Chim. Acta* **1965**, *3*, 211.

(12) (a) Cotton, F. A.; Haas, T. E. *Inorg. Chem.* **1964**, *3*, 10. (b) Grossman, C. D.; Olsen, D. P.; Duffey, C. H. *J. Chem. Phys.* **1963**, *38*, 73. (c) Guggenberger, L. J.; Sleight, A. W. *Inorg. Chem.* **1969**, *8*, 2041. (d) Cotton, F. A.; Stanley, G. G. *Chem. Phys. Lett.* **1978**, *58*, 450. (e) Hughbanks, T.; Hoffmann, R. *J. Am. Chem. Soc.* **1983**, *105*, 1150.

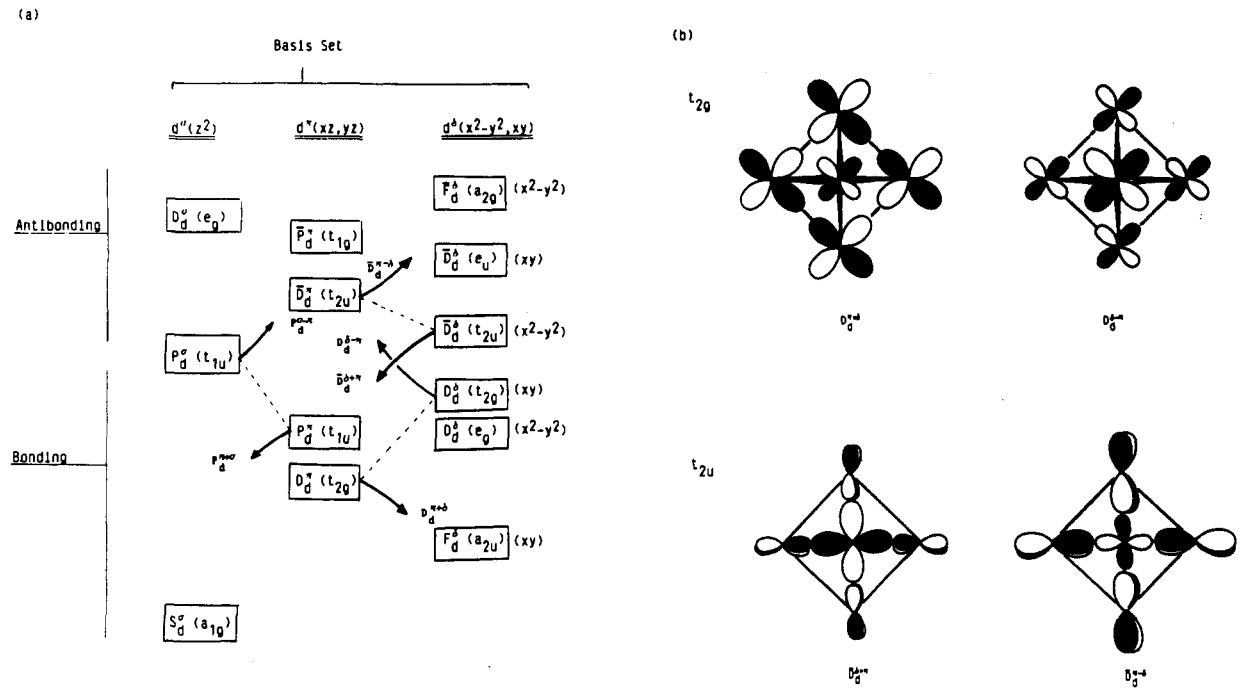

Figure 2. (a) Mixing of d-band orbitals, with the same symmetry, for a "naked" Mo_6 octahedral custer. The orbitals are labeled according to which atomic orbitals they are derived from. (b) Effect of π/δ mixing on the d-band t_{2g} and t_{2u} orbitals.

direct link between the polyhedral geometry and the total number of valence electrons, i.e. $14n + 2$ for closo, $14n + 4$ for nido, and $14n + 6$ for arachno.[2] This structural relationship arises because the number of bonding skeletal molecular orbitals remains constant in a series of related closo, nido, and arachno polyhedral molecules.[2] In clusters with π-donor ligands a similar family of structures has been observed[13] (see III–VI for example), but these compounds do not show a similar simple electronic relationship.

The strategy for the present analysis is first to evaluate the effect of introducing terminal, edge- and face-bridging π-donor ligands into the bonding scheme developed for a bare octahedral metal cluster. The differences between π-donor and π-acceptor ligands will then be highlighted by a comparison of related carbonyl and chloride clusters. The Stone approach[5] is used to describe the nodal characteristics of the molecular orbitals of the naked metal clusters and the linear combinations of the ligand orbitals. In this way the clusters are treated as a series of concentric spheres on which are placed the metal atoms and the bridging and terminal ligands. The second aim is to account for the electronic structures of closo, nido, and arachno clusters based on the octahedron with π-donor ligands. This provides a basis not only for accounting for some of the clusters of this type that have been reported, but also for predicting new clusters.

Results and Discussion

Figure 1 illustrates the relative energies of the molecular orbitals in a "naked" Mo_6 octahedral cluster.[3a,14] The molybdenum 5s and 5p orbitals generate a spectrum of molecular orbitals with a large energy spread, although as Woolley has pointed out this is not synonomous with strong metal–metal bonding through the s and p orbitals.[15] A crucial feature of this spectrum of molecular orbitals is the occurrence of 11 strongly antibonding molecular orbitals, viz. D_{sp}^{σ} (e_g), P_p^{π}–P_{sp}^{σ} (t_{1u}), $\bar{P}_p^{\pi}$ (t_{1g}), and $\bar{D}_p^{\pi}$ (t_{2u}) (Figure 1), which are unsuitable for either metal–metal bonding or metal–ligand bonding by virtue of their antibonding metal–metal character and their hybridization toward the center of the cluster. These are present not only for naked molybdenum clusters, but also for clusters of the later transition metals.[16] More generally, it has been established that deltahedral clusters have $2n - 1$ "inaccessible" molecular orbitals of this type, and therefore if all of the remaining metal valence orbitals are utilized in metal–ligand and metal–metal bonding, such clusters are characterized by $14n + 2$ valence electrons ($4n + 2$ valence electrons for clusters based on main-group atoms without d valence orbitals).

Since the octahedral π-donor clusters, e.g. I and II, have fewer valence electrons than that predicted on the basis of the 11 inaccessible molecular orbitals derived from the s and p orbitals, it can be concluded that such clusters have additional inaccessible orbitals derived from the metal d valence orbitals. The spectrum of molecular orbitals derived for the 4d orbitals in Figure 1 is relatively narrow (ca. 4.0 eV) and has 13 bonding and 17 antibonding components. The atomic characteristics and symmetries of these molecular orbitals are illustrated in more detail in Figure 2a. The symmetry-allowed mixings of the σ, π, and δ components of the d band are also shown in this figure. The π/δ mixings are particularly important for understanding the electronic structures of the π-donor clusters and are illustrated schematically in Figures 2a and 2b. The δ orbitals have been labeled according to whether they have been derived from linear combinations of $d_{x^2-y^2}$ or d_{xy} metal atomic orbitals. The former are defined so that their lobes point along the edges, and the latter toward the faces of the octahedron. It follows that these molecular orbitals interact in a highly specific and complementary manner with edge- and face-bridging ligands. As a result of the π/δ mixings illustrated in Figures 2a and 2b, the molybdenum $d_{x^2-y^2}$ orbitals generate only one strongly antibonding skeletal molecular orbital ($\bar{F}_d^{\delta}$ (a_{2g})) (**1**).

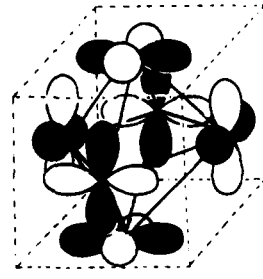

$\bar{F}_d^{\delta}$ (a_{2g})

1

(13) (a) Jodden, K.; Schnering, H. G.; Schafer, H. *Angew. Chem., Int. Ed. Engl.* **1975**, *14*, 570. (b) Chisholm, M. H.; Errington, R. J.; Folting, K.; Huffman, J. C. *J. Am. Chem. Soc.* **1982**, *104*, 2025. (c) Stensvad, S.; Helland, B. J.; Bakich, M. W.; Jacobson, R. A.; McCarley, R. E. *J. Am. Chem. Soc.* **1978**, *100*, 6257.

(14) (a) Burdett, J. K.; Lin, J.-H. *Inorg. Chem.* **1982**, *21*, 5. (b) Tatewaki, H.; Miyoshi, E.; Nakemura, T. *J. Chem. Phys.* **1982**, *76*, 5073.

(15) Woolley, R. G. *Nouv. J. Chim.* **1981**, *5*, 219, 227.

(16) Mingos, D. M. P. *J. Chem. Soc., Dalton Trans.* **1974**, 133.

The $\bar{D}_d^{\delta}$ (t_{2u}) molecular orbital has been stabilized by mixing with the higher lying $\bar{D}_d^{\pi}$ (t_{2u}) molecular orbital. In contrast, the d_{xy} orbitals generate five $\bar{D}_d^{\delta}$ (e_u) (**2**) and D_d^{δ} (t_{2g}) antibonding mo-

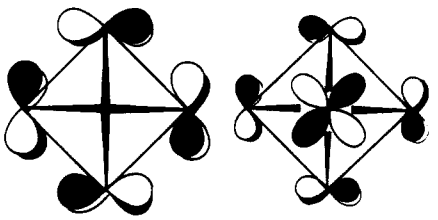

$\bar{D}_d^{\delta}$ (e_u)

2

lecular orbitals. The antibonding character of the latter is introduced by substantial mixing with the lower lying D_d^{π} (t_{2g}) orbital, as shown in Figure 2b. It is these antibonding molecular orbitals derived from the d^{δ} atomic orbitals that provide an explanation for the presence of additional inaccessible molecular orbitals in π-donor clusters. However, a clear exposition of the manner in which this is achieved requires a further analysis of the bonding in the hypothetical clusters $[Mo_6H_{14}]$ and $[Mo_6H_{18}]$, which have hydrido ligands capable only of interacting in a σ fashion with the cluster orbitals.

Hydrido-Bridged Clusters. In $[Mo_6H_{14}]$ and $[Mo_6H_{18}]$ the six terminal hydrido ligands generate a_{1g}, t_{1u}, and e_g linear combinations, which interact primarily with the out-pointing and matching set of cluster MO's derived from Mo 5s and 5p (set 2 in Figure 1). In $[Mo_6H_{14}]$, the eight face-bridging ligands define a cube and their linear combinations span the representations S^{σ} (a_{1g}), P^{σ} (t_{1u}), D^{σ} (t_{2g}), and F^{σ} (a_{2u}). In $[Mo_6H_{18}]$ the 12 edge-bridging ligands span the representations S^{σ} (a_{1g}), P^{σ} (t_{1u}), D^{σ} (t_{2g} and e_g), and F^{σ} (t_{2u}). The hydrogen 1s orbitals of the bridging ligands have no angular nodes, and consequently the linear combinations listed above overlap most effectively with the cluster MO's that are also not noded across either the edges or faces of the polyhedron. The seven bonding skeletal molecular orbitals derived from the metal s and p atomic orbitals (set 3 in Figure 1) represent the most suitable match, but there remain some linear combinations that do not find such a match, i.e. F^{σ} (a_{2u}) (**3**) in

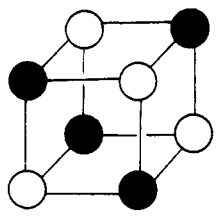

F_x^{σ} (a_{2u})

3

$[Mo_6H_{14}]$ and D^{σ} (e_g) and F^{σ} (t_{2u}) (**4**) in $[Mo_6H_{18}]$. These linear

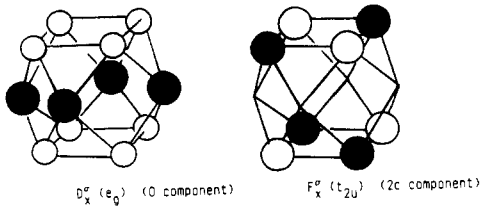

D_x^{σ} (e_g) (O component) F_x^{σ} (t_{2u}) (2c component)

4

combinations possess two angular nodes that pass through the vertices of the octahedron and are therefore matched by metal cluster MO's derived from the d^{δ} band, i.e. F_d^{δ} (a_{2u}, xy) (**5**) in $[Mo_6H_{14}]$ and D_d^{δ} (e_g, $x^2 - y^2$) (**6**) and $\bar{D}_d^{\delta+\pi}$ (t_{2u}, $x^2 - y^2$) in

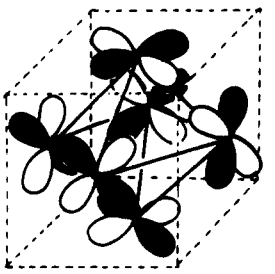

F_d^{δ} (a_{2u})

5

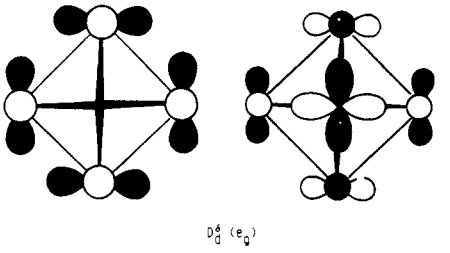

D_d^{δ} (e_g)

6

$[Mo_6H_{18}]$. The disposition of the ligands relative to the edges and faces of the octahedron decides the choice of linear combinations derived either from d_{xy} or $d_{x^2-y^2}$.

The formation of molecular orbitals from the linear combinations described above leaves a d band of 29 orbitals for $[Mo_6H_{14}]$ (12 bonding and 17 antibonding) and 25 orbitals for $[Mo_6H_{18}]$ (8 bonding and 17 antibonding). If these molecular orbitals and the cluster hydrogen-bonding molecular orbitals were completely filled, the resultant electron count for both clusters would be 86, i.e. the same as that for carbonyl clusters, but the net metal–metal bonding would be negligible because the occupation of the antibonding d-band molecular orbitals cancels the bonding effects in the lower lying molecular orbitals. The computed Mulliken overlap populations[17] for these hypothetical 86-electron clusters [−0.04 ($[Mo_6H_{14}]$) and +0.02 ($[Mo_6H_{18}]$)] confirm this conclusion.

π-Donor and π-Acceptor Clusters. By definition π-donor and π-acceptor bridging ligands have additional atomic orbitals with nodal planes perpendicular to the ligand–metal bond directions. They generate linear combinations that match MO's derived from the d band that are also noded across the edges and faces of the octahedron. These noded MO's are associated with the antibonding components of the d band. For example, in the face-bridged cluster $[Mo_6X_{14}]$ the ligand π-orbitals match the symmetries and nodal characteristics of 16 of the 17 antibonding d-band MO's described above for $[Mo_6H_{14}]$. The only orbital that does not find a match is $\bar{F}_d^{\delta}$ (a_{2g}, $x^2 - y^2$) (**1**), which is doubly noded across the faces of the octahedron. If X is a π-acceptor, the resultant effect is the stabilization of these 16 antibonding d band molecular orbitals, by the transfer of electron density to the π^*(CO) molecular orbitals. The $\bar{F}_d^{\delta}$ (a_{2g}) MO alone is not stabilized by back-donation effects, and whether it is characterized as "inaccessible" or not depends on the inherent bandwidth of the d molecular orbitals. For a later first-row transition metal, the d bandwidths are not large and consequently this molecular orbital is not sufficiently strongly antibonding to achieve the status of "inaccessible". Therefore, in clusters such as $[Co_6(CO)_{14}]^{4-}$,[18] this MO is occupied and the total electron count is 86. In transition-metal carbonyl clusters this molecular orbital can be stabilized also by bridge–terminal ligand rearrangements. For example, in $[Os_6(CO)_{18}]^{2-}$,[19] this orbital is stabilized by overlap with

(17) Mulliken, R. S. *J. Chem. Phys.* **1955**, *23*, 1833, 2343.
(18) Albano, V.; Bellon, P. L.; Scatturin, V. *J. Organomet. Chem.* **1969**, *16*, 461.
(19) Johnson, B. F. G.; Lewis, J. *Adv. Inorg. Chem. Radiochem.* **1981**, *24*, 225.

a matching linear combination of π^* (CO) orbitals of the conical $M(CO)_3$ fragments.

If X is a π-donor, e.g. Cl, the 16 linear combinations of Cl $3p^\pi$ orbitals are more stable than the d-band orbitals and their overlap leads to a set of 16 bonding molecular orbitals localized mainly on the ligands. This represents in effect a replacement of 16 antibonding metal–metal d-band orbitals by a matching set of 16 orbitals localized predominantly on the ligand. This effective removal of the antibonding components of the d band leads to a strengthening of the metal–metal bonds relative to the situation in the hydrido clusters. This is reflected by an increase in the calculated overlap population to +0.28. The $\bar{F}_d^\delta$ (a_{2g}) MO is unaffected by these interactions, and therefore the situation is strictly analogous to that described above for π-acceptor clusters. However, for an early transition metal such as Mo the d–d overlaps are much larger than those for Co and a_{2g} MO is substantially more antibonding and takes on the status of an inaccessible MO. Therefore, clusters of this type are characterized by 84 rather than 86 valence electrons.

In $[Mo_6X_{18}]$ the π-orbitals of the bridging ligands no longer interact with the metal orbitals in an equivalent fashion. The π-orbitals lying parallel to the octahedral edges (**7a**) overlap more

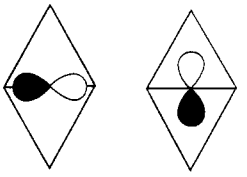

7a **7b**

strongly with the metal orbitals than those perpendicular (**7b**). The 12 $\pi_\parallel$ orbitals interact primarily with matching antibonding components of the d band, which are also noded across the edges. The remaining 5 antibonding components of the d band, $\bar{D}_d^\delta$ (e_u, xy) and $D_d^{\pi-\delta}$ (t_{2g}, xy), are unaffected by the ligand $\pi_\parallel$ orbitals but experience a smaller secondary interaction with the $\pi_\perp$ linear combinations with matching symmetry characteristics. If X is a π-acceptor ligand, then the result is a substantial stabilizing effect for 12 components of the d band and a lesser stabilization for the remaining 5 antibonding components. Occupation of these molecular orbitals leads to a total valence electron count of 86 and a strengthening of the metal–metal bonding interactions. If X is a π-donor ligand, the 12 orbitals that are now localized predominantly on the ligand arise from the bonding interactions of the ligand $\pi_\parallel$ orbitals with the cluster orbitals. The remaining five components of the antibonding part of the d band ($\bar{D}_d^\delta$ (e_u) and $D_d^{\pi-\delta}$ (t_{2g})) assume the status of inaccessible if the d–d overlap integrals are large, i.e. for second- or third-row early transition metals. The inaccessible nature of these orbitals is enhanced by weak antibonding interactions with the ligand $\pi_\perp$ orbitals. The presence of these additional inaccessible molecular orbitals accounts for the 76 electron count observed for example in $[Nb_6Cl_{18}]^{4-}$. The enhanced strength of the metal–metal bonding in such clusters, which results from the transfer of electron density from antibonding components of the d band to orbitals localized on the ligands, is confirmed by a computed Mo–Mo overlap population of +0.34 for $[Mo_6Cl_{18}]^{2+}$.

The detailed analysis given above has emphasized the important role played by the metal d^δ orbitals in influencing the total number of MO's available for metal–metal and metal–ligand bonding. Figure 3 illustrates the relative energies of the molecular orbitals derived from d_{xy} and $d_{x^2-y^2}$. The molecular orbitals are interrelated by what Stone has described as a parity transformation operation.[5a] This operation, which rotates each atomic orbital by 45° about the radius vector of the polyhedron, interconverts each d_{xy} orbital into $d_{x^2-y^2}$ and an L_d^δ molecular orbital into its $\bar{L}_d^\delta$ counterpart. The following molecular orbitals are related in this fashion:

$$\bar{D}_d^\delta\ (t_{2u}, x^2-y^2) \leftrightarrow D_d^\delta\ (t_{2g}, xy)$$

$$D_d^\delta\ (e_g, x^2-y^2) \leftrightarrow \bar{D}_d^\delta\ (e_u, xy)$$

$$F_d^\delta\ (a_{2u}, xy) \leftrightarrow \bar{F}_d^\delta\ (a_{2g}, x^2-y^2)$$

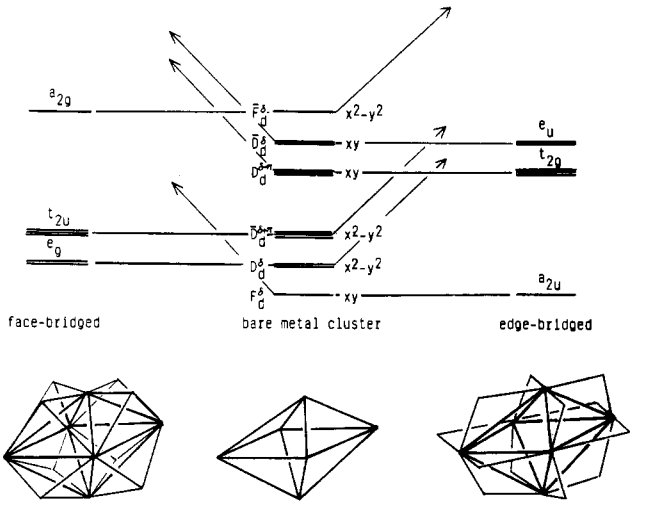

Figure 3. Representation of the complementary effects of edge- and face-bridging (σ- and π-donor) ligands on "naked" octahedral cluster orbitals with mainly d^δ character. The arrows represent the utilization of d^δ orbitals in bonding to the bridging ligands.

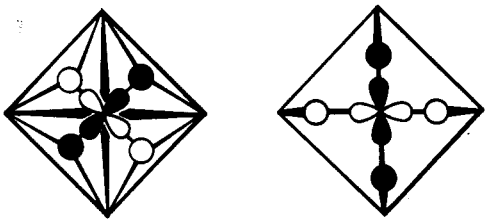

(a) $d_{xy}+\delta(X_4)$ (b) $d_{x^2-y^2}+\delta(X_4)$

Figure 4. Bonding interaction of d^δ atomic orbitals of a metal vertex with δ-symmetry combinations of "σ-donor" orbitals $\delta(X_4)$ in (a) face-bridging and (b) edge-briding sites.

The parity transformation also interchanges the bonding and antibonding character of the MO's (see Figure 3, for example). The face- and edge-bridging ligands form four localized metal–ligand bonds to each metal atom. These bonds form a square plane and necessitate the use of one of the d^δ pair (xy or x^2-y^2) on each metal atom to form the coordinate bonds.[12a] These interactions are illustrated in Figure 4.

Once half of the d^δ orbitals have been utilized in this fashion, the spectrum of the remaining orbitals determines the electron count in these π-donor clusters. In the face-bridged cluster there remains only one strongly antibonding δ-orbital ($\bar{F}_d^\delta$ (a_{2g})), which assumes the designation of inaccessible for early transition metals where the d–d antibonding interactions are relatively strong. In consequence $[Mo_6Cl_{14}]^{2-}$ has 12 inaccessible orbitals and an electron count of 84. In the edge-bridged clusters there are 5 high-lying antibonding δ-orbitals ($\bar{D}_d^\delta$ (e_u (**2**) and $D_d^{\pi-\delta}$ (t_{2g})), which for an early transition metal are inaccessible. For such a cluster there are in total 16 inaccessible orbitals and a resultant electron count of 76, e.g. $[Nb_6Cl_{18}]^{4-}$. Although it has become customary to discuss the bonding in π-donor and π-acceptor clusters separately, the analysis presented above demonstrates clearly how closely related the two classes of clusters are. In both classes of octahedral clusters the ligands serve to transfer electron density from antibonding components of the d band. Both classes of clusters have 11 inaccessible orbitals derived from the metal s and p orbitals. However, for the earlier transition metals further inaccessible orbitals arise from the antibonding components of the d^δ band because of their greater antibonding character. The number of inaccessible orbitals of this type depends on the position of the ligands relative to d_{xy} and $d_{x^2-y^2}$.

Nido and Arachno π-Donor Clusters. Examples of nido and arachno clusters derived from $[Mo_6Cl_{14}]^{2-}$ are illustrated in III–VI, and their electronic characteristics are summarized in Table I.[16]

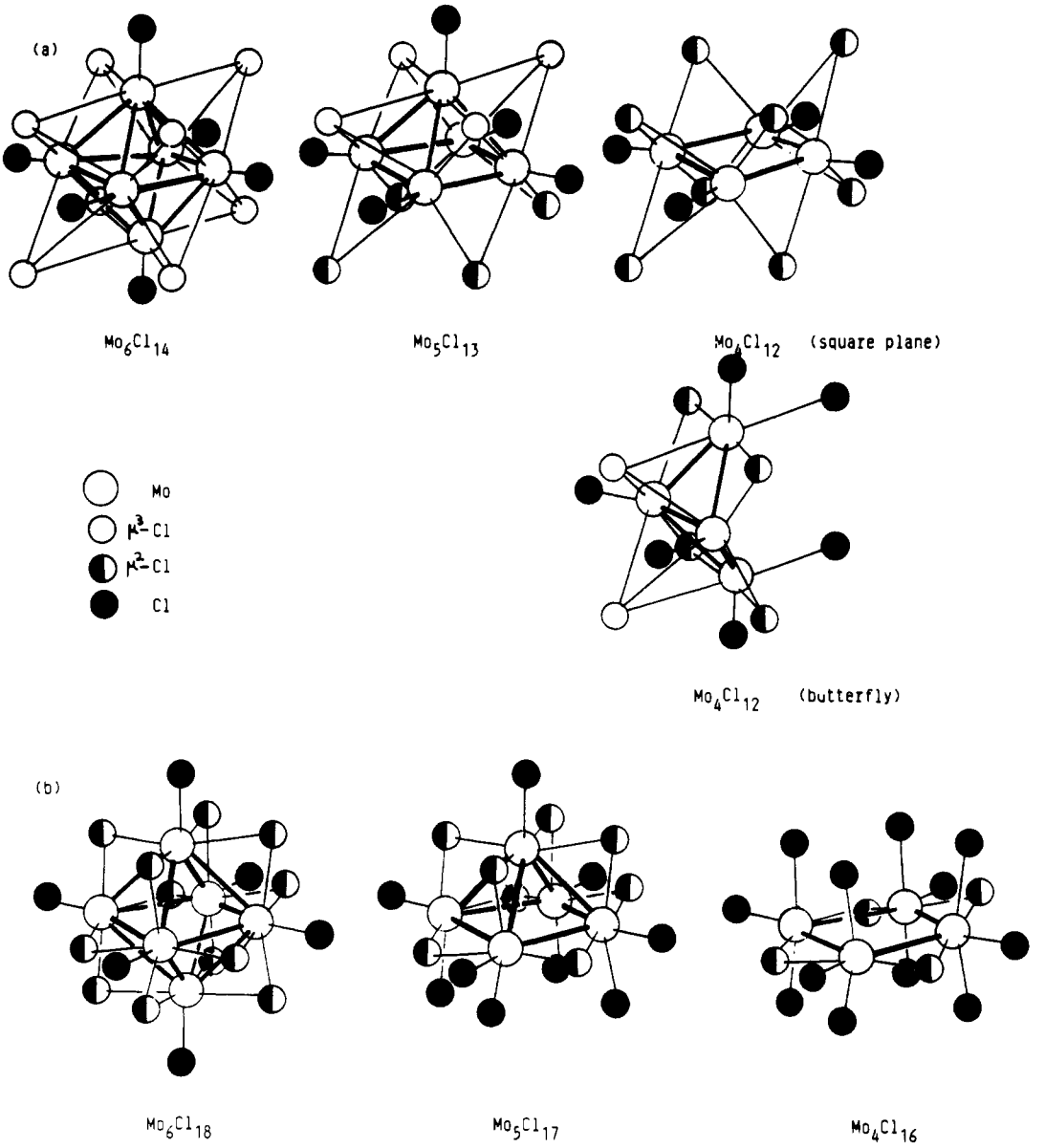

Figure 5. Closo, nido, and arachno chloride-bridged clusters based on (a) $[Mo_6Cl_{14}]$ and (b) $[Mo_6Cl_{18}]$.

Table I. Nido and Arachno Clusters Based on Face-Bridged Octahedral Mo_6X_{14} (X = Cl, Br, I, or O-*i*-Pr)

cluster	structure	no. of cluster valence of electrons	ref
$[Mo_5Cl_{13}]^{2-}$	square pyramid	69	12a
$[Mo_4(O\text{-}i\text{-}Pr)_8Cl_4]$	square plane	52	12b
$[Mo_4(O\text{-}i\text{-}Pr)_8Br_4]$	butterfly	52	12b
$[Mo_4I_{11}]^{2-}$	butterfly	55	12c

For completeness we have also performed molecular orbital calculations on the nido and arachno derivatives of $[Mo_6Cl_{18}]^{2+}$ illustrated in Figure 5 although such compounds have not actually been characterized to date. One obvious difference between π-acceptor and π-donor cluster compounds of this type is the change in electron-donating characteristics of the bridging ligands that result from the removal of a metal vertex. For example, the removal of a metal vertex adjacent to a face-bridging chloride (5-electron donor) generates an edge-bridging chloride (3-electron donor). Similarly, the removal of a metal atom adjacent to a bridging chloride generates a terminal chloride (1-electron donor). For carbonyl clusters a similar pattern is not observed since this ligand generally functions as a 2-electron donor independent of the number of metal atoms bridged. Although the loss of metal vertices illustrated in Figure 5 alters the coordination number and electron-donating characteristics of the individual ligands, their overall cubic or cuboctahedral arrangement around the cluster is retained.

A comparison of the frontier molecular orbitals for octahedral (*closo*-) $[Mo_6Cl_{14}]^{2-}$ and square-planar (*arachno*-) $[Mo_4Cl_{12}]$ is given in Figure 6. The molecular orbitals of the intermediate *nido*-$[Mo_5Cl_{13}]$ cluster are also illustrated in this figure. When two trans vertices are removed, the HOMO in $[Mo_6Cl_{14}]^{2-}$ (D_d^{δ} (e_g)) generates one strongly antibonding component (b_{1g}) while the second component remains essentially unaffected (a_{1g}). The former is doubly noded in the M_4 plane and strongly antibonding since the nodes pass through the metal–metal vectors. In the octahedral cluster the antibonding nature of this orbital is mitigated by overlap with an in-phase (δ) combination of $d_{x^2-y^2}$ orbitals on the axial atoms as shown in Figure 7a. The a_{1g} component of D_d^{δ} (e_g) has no contribution from the axial atoms, and therefore its energy remains essentially unaffected by the removal of the axial metal atoms.

The $\bar{D}_d^{\delta+\pi}$ (t_{2u}) octahedral orbitals give rise to b_{2u} and e_u components. The b_{2u} orbital is strongly antibonding because it is doubly noded in the M_4 plane, but it is stabilized in the octahedron by overlap with an out-of-phase (δ^*) combination of $d_{x^2-y^2}$ orbitals on the axial atoms (see Figure 7b). The e_u orbitals are not as strongly antibonding because they possess only a single node in the M_4 plane. In the octahedron these orbitals are stabilized by an in-phase (π) combination of d_{xz} and d_{yz} orbitals on the axial

Table II. Calculated Mo–Mo Overlap Populations for Clusters Based on $[Mo_6Cl_{14}]^{2-}$ and $[Mo_6Cl_{18}]^{2-}$

cluster	structure	no. of cluster valence electrons	no. of skeletal electrons	calcd Mo–Mo overlap popln
$[Mo_6Cl_{14}]^{2-}$	octahedron	84	24	+0.28[a]
$[Mo_5Cl_{13}]^{-}$	square pyramid	68	18	+0.29,[b] +0.34[c]
$[Mo_4Cl_{12}]$	square plane	52	12	+0.44
$[Mo_6Cl_{18}]^{2+}$	octahedron	76	16	+0.34
$[Mo_5Cl_{17}]^{3-}$	square pyramid	66	16	+0.35,[b] +0.46[c]
$[Mo_4Cl_{16}]^{8-}$	square plane	56	16	+0.58

[a] The Mo–Mo overlap population for the 84-electron $[Mo_6(CO)_{14}]^{20-}$ cluster is 0.18, reflecting the less complete transfer of electron density from the metal–metal antibonding levels to the ligands. [b] Apical–basal. [c] Basal–basal.

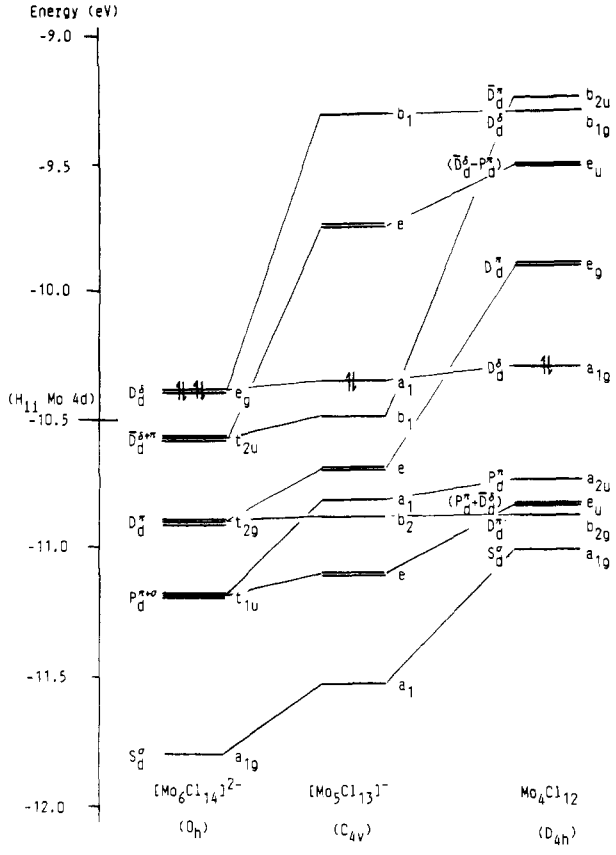

Figure 6. Molecular orbital correlation diagram for the removal of one or two (trans) MoCl fragments from $[Mo_6Cl_{14}]^{2-}$. The effect of decapping on the d-band bonding orbitals of the parent close cluster is shown.

atoms. Figure 7c illustrates this and also the change in character of the e_u pair due to mixing with the lower lying $P_d^{\pi+\sigma}$ (e_u) orbitals, which have predominantly π-character. This mixing serves to increase the antibonding character of these orbitals. Figure 6 suggests that the removal of two vertices results in the destabilization of an e_g pair of orbitals derived from D_d^{π} (t_{2g}) set of the octahedron. The e_g orbitals are weakly antibonding due to the single node that they posses in the M_4 plane. In the octahedron they are stabilized by overlap with out-of-phase (π^*) combinations of d_{xz} and d_{yz} orbitals on the axial atoms (see Figure 7d). The remaining component (b_{2g}) derived from the t_{2g} set retains its bonding character on decapping, since it has no contribution from the capping atoms. It is also doubly noded in the M_4 plane, but the nodes pass through the metal atoms (Figure 7)), so their bonding character is retained. Finally, inspection of Figure 6 reveals that the square-planar cluster possesses 6 d-band bonding molecular orbitals (6 of the original 12 bonding orbitals of the octahedral cluster having become antibonding on decapping). This leads to the prediction of a 52-electron $[M_4Cl_{12}]$ cluster. Although such a cluster has not been isolated, isoelectronic and isostructural $[Mo_4(O\text{-}i\text{-}Pr)_8Cl_4]$ (IV) has been structurally characterized.[13b] In the intermediate case of the nido square-pyramidal cluster (see Figure 6) the six molecular orbitals corresponding to the destabilized orbitals of the square-planar cluster transform as two b_1 orbitals and 2-e pairs under the lower (C_{4v}) symmetry. Mixing occurs that results in the formation of three bonding (b_1 + e) and three antibonding (b_1 + e) orbitals. The bonding combinations have π or δ contributions from the remaining capping atom that stabilize the doubly or singly noded orbitals, respectively. In the antibonding components these stabilization effects are absent. Electron occupation of the nine-band bonding molecular orbitals leads to the prediction of a stable 68-electron $[Mo_5Cl_{13}]^{-}$ square-pyramidal cluster. The actual cluster isolated has an additional electron, i.e. $[Mo_5Cl_{13}]^{2-}$ (III),[13a] and our calculations indicate that the additional electron resides in an orbital of e symmetry, which is singly noded and weakly antibonding in the square plane.

To summarize the results above, the octahedral cluster is characterized by 12 metal–metal bonding molecular orbitals and its nido and arachno derivatives are characterized by 9 and 6 bonding MO's, respectively (i.e. $3n - 6$ where n is the number of metal atoms). Removing a vertex results in the loss of three bonding molecular orbitals, and the number of polyhedral edges decreases by four. Therefore, the ratio of bonding orbitals to edges increases. This is reflected in an increase in the computed metal–metal overlap populations (see Table II) and a decrease in metal–metal bond lengths. The Mo–Mo bond lengths in $[Mo_5Cl_{13}]^{2-}$ (2.602 Å apical–basal and 2.563 Å basal–basal) are shorter than those in octahedral $[Mo_6Cl_{14}]^{2-}$ (2.610 Å). The square-planar cluster $[Mo_4(O\text{-}i\text{-}Pr)_8Cl_4]$ has even shorter Mo–Mo bond lengths (2.378 Å).

The 52-valence-electron cluster $[Mo_4(O\text{-}i\text{-}Pr)_8Br_4]$ (V)[13b] has a butterfly, C_{2v}, geometry that is an alternative arachno geometry derived from the octahedron by the loss of two cis metal atoms. This cluster has 12 d-band bonding electrons in an analogous fashion to that described above for the square-planar cluster. The metal–metal bonds are also short in this cluster (average 2.50 Å). A 55-electron butterfly cluster, $[Mo_4I_{11}]^{2-}$ (VI) has also been structurally characterized, but it has a slightly different arrangement of bridging ligands. Instead of having eight ligands arranged in a cubic fashion, it has only six and the remaining ligand is located at the midpoint of the edge connecting the missing bridging ligands; see **8**. This ligand bridges the wing tips of the

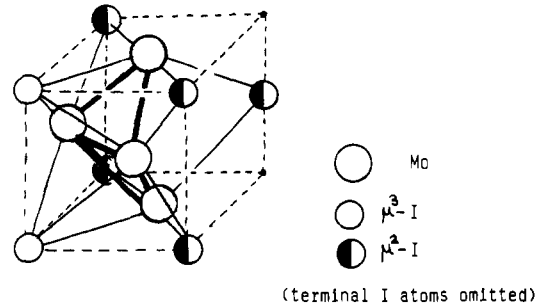

8

butterfly and causes a compression leading to a wing tip separation of 3.035 Å rather than the 3.287 Å separation observed in the 55-electron cluster.

Figure 8 illustrates the effect of metal–ligand interactions on the frontier orbitals of a bare Mo_4 cluster with a butterfly geometry. In $[Mo_4Cl_{12}]$ and $[Mo_4Cl_{11}]$, with the appropriate wing tip separations, the frontier orbitals of particular interest are b_1,

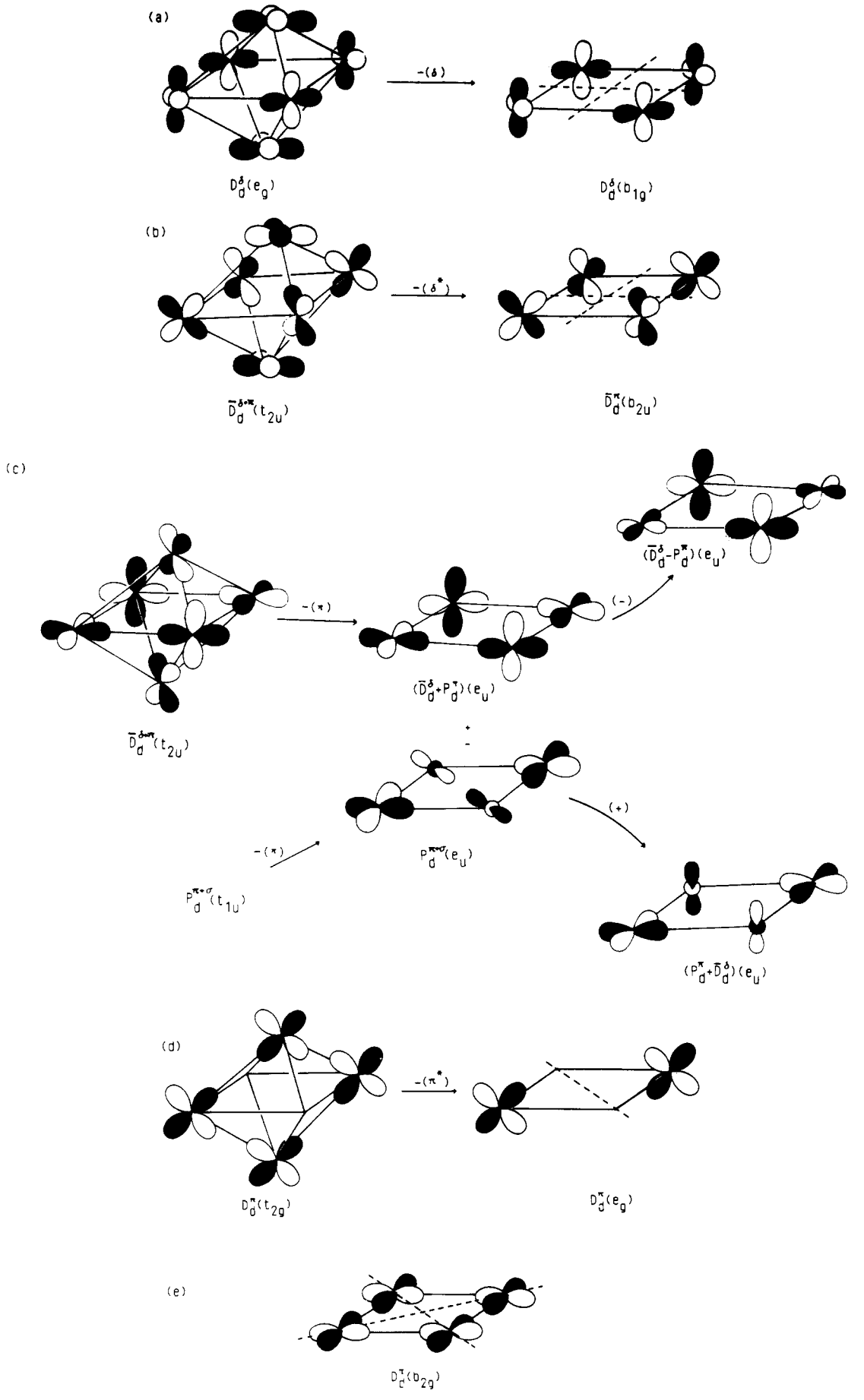

Figure 7. Loss of stabilizing overlap with (in-phase or out-of-phase) combinations of d^{π} and d^{δ} orbitals on the axial atoms on going from octahedral $[Mo_6Cl_{14}]$ to square-planar $[Mo_4Cl_{12}]$.

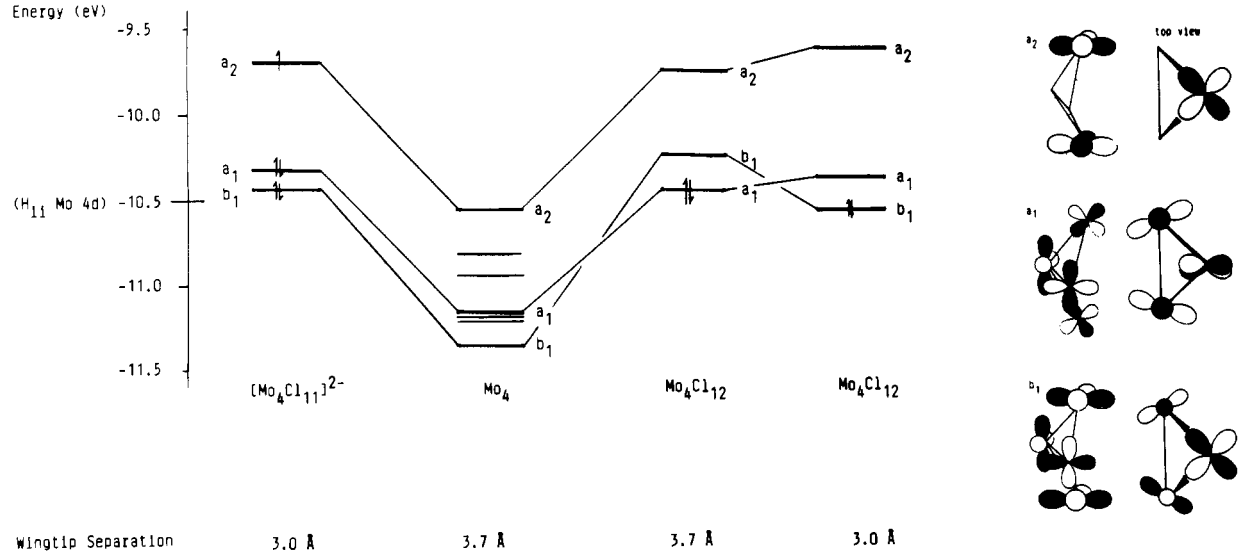

Figure 8. Correlation of molecular orbitals of a "naked" Mo_4 butterfly cluster with those of $[Mo_4Cl_{11}]$ and $[Mo_4Cl_{12}]$. Also shown is the effect of decreasing the wing tip separation in Mo_4Cl_{12}. Attention is focussed on the b_1, a_1, and a_2 orbitals of Mo_4, which constitute the major components of the frontier orbitals of the bridged clusters.

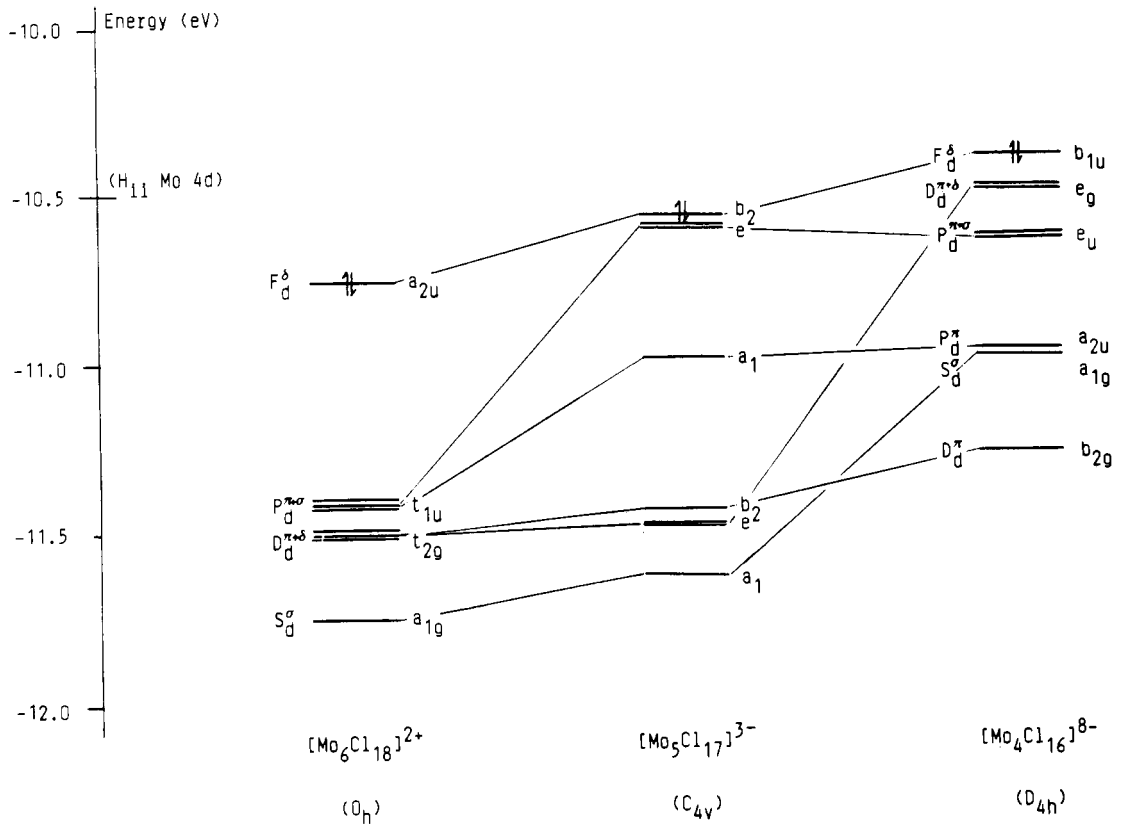

Figure 9. Molecular orbital correlation diagram for the removal of one or two (trans) MoCl fragments from $[Mo_6Cl_{18}]^{2+}$. Only those cluster bonding orbitals of predominantly d character are shown.

a_1, and a_2. The b_1 orbital is mainly localized on the wing tip atoms, with a d^δ bonding interaction between them. Consequently, this orbital is stabilized as the cluster is compressed. $[Mo_4Cl_{12}]$ with 12 electrons in the d band has the configuration $(a_1)^2(b_1)^0(a_2)^0$, while the 15-electron $[Mo_4Cl_{11}]^{2-}$ cluster has the configuration $(b_1)^2(a_1)^2(a_2)^1$. The unpaired electron therefore resides in an orbital of a_2 symmetry (see Figure 8) that is weakly antibonding between the wing tip atoms. These results agree qualitatively with those suggested by McCarley.[13c]

When the observed bond lengths in the 52- and 55-electron clusters are compared, the wing tip hinge metal–metal distances are very similar (average 2.515 Å for the 52-electron cluster and 2.542 Å for the 55-electron cluster). There is, however, a significant increase in the length of the hinge bond (2.481 Å in the 52-electron cluster and 2.669 Å in the 55-electron cluster). This is consistent with the occupation, in the latter, of the b_1 orbital shown in Figure 8 that has a σ antibonding component between the hinge atoms.

The effect of removing axial cluster vertices from the edge-bridged $[Mo_6Cl_{18}]$ cluster is illustrated in Figure 9. In this case the number of bonding skeletal molecular orbitals remains constant (8) on decapping. From Figure 9 it is apparent that the F_d^δ (a_{2u}) orbital is destabilized only slightly on decapping. This results from the loss of overlap with the out-of-phase (δ^*) combination of d_{xy} orbitals on the axial atoms, as shown in Figure 10a. This orbital is doubly noded in the equatorial plane, but the nodes pass through

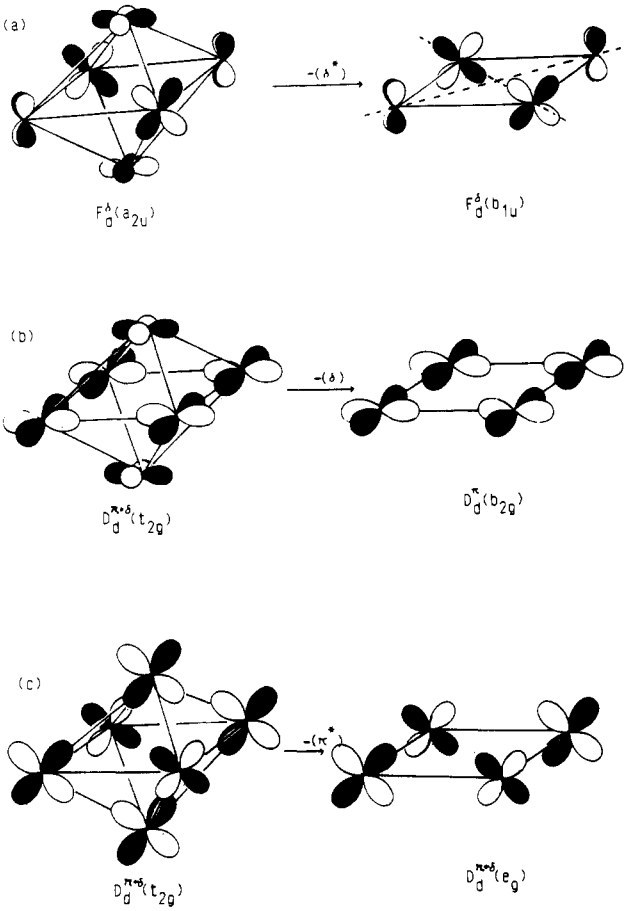

Figure 10. Loss of stabilizing overlap with (in-phase or out-of-phase) combinations of d^{π} and d^{δ} orbitals on the axial atoms on going from octahedral Mo_6Cl_{18} to square-planar Mo_4Cl_{16}.

the atoms and the orbital is overall bonding. This b_{1u} orbital therefore remains bonding on decapping to form the arachno cluster. The octahedral $D_d^{\pi+\delta}$ (t_{2g}) orbitals split on decapping to give b_{2g} and e_g orbitals in the square-planar cluster. Removing the capping atoms destabilizes the b_{2g} component due to loss of overlap with the in-phase combination (δ) of d_{xy} orbitals on the axial atoms (see Figure 10b). The e_g components are destabilized also as a result of overlap with the out-of-phase (π^*) combinations of d_{xz} and d_{yz} orbitals on the departing axial atoms (see Figure 10c). However, these orbitals remain sufficiently low lying for electron occupation, due to π/δ mixing in the square plane. This mixing is absent in the face-bridged cluster because the δ-component is removed as a consequence of bonding interactions with the bridging ligands.

The occupation of the metal–ligand bonding MO's and 8 d-band molecular orbitals leads to predicted electron counts of 66 for the square-pyramidal cluster $[Mo_5Cl_{17}]^{3-}$ and 56 for a square-planar $[Mo_4Cl_{16}]^{8-}$ cluster, although $[Re_4Cl_{16}]^{4-}$ may represent a more reasonable synthetic goal for the latter. Since there is no change in the number of M–M bonding molecular orbitals in this series of closo, nido, and arachno clusters, they resemble more closely the situation in metal carbonyl cluster and borane polyhedral molecules.[2] The Mo–Mo overlap populations (see Table II) suggest a strengthening in metal–metal bonding as the number of metal atoms is reduced.

The different behavior of face- and edge-bridged clusters described above can be explained in a simple fashion with localized bonding schemes. The metal–metal bonding in the edge-bridged clusters can be represented in terms of eight face-localized three-center two-electron bonds. Removing a metal atom leads to a pyramidal cluster with the same number of edges as its precursor had faces which can be described also in terms of a localized bonding scheme involving eight two-center two-electron bonds. Figure 11 shows how a face-capping orbital becomes edge

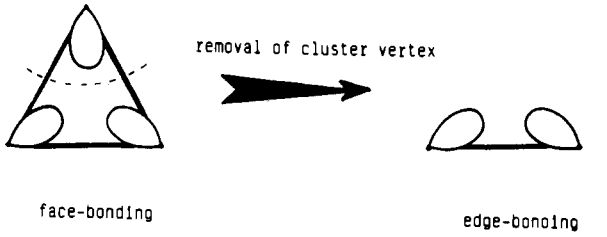

Figure 11. Conversion of a localized face-bonding cluster molecular orbital into an edge-bonding orbital by the removal of a metal vertex.

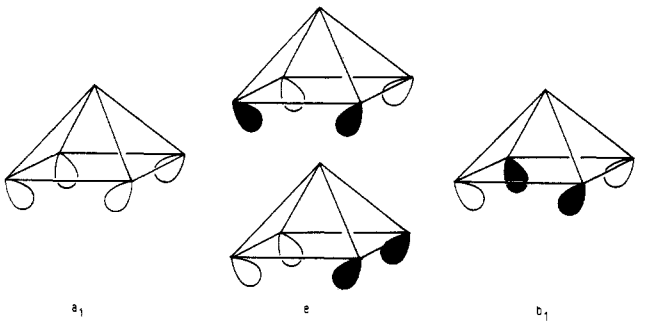

Figure 12. Localized bonding orbitals on the square face formed by removing a metal vertex from the face-bridged cluster. Only the nodeless a_1 orbital is sufficiently bonding to be occupied.

bonding when a vertex is removed. When two trans metal atoms are removed from the octahedron, the bonding in the resultant ring cluster can be described in terms of formal double bonds between the metal atoms. Since the ring has half the edges of the parent octahedron, this localized description leads to the same number of orbitals in total. An examples of such a double-bonded cluster is $[Re_3Cl_{12}]^{3-}$ (VII),[20] which has six sep's and may be

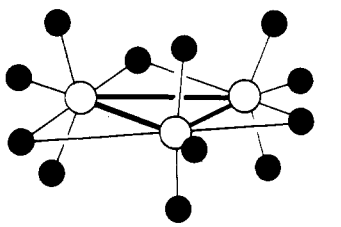

$[Re_3Cl_{12}]^{3-}$

(VII)

regarded as an arachno trigonal bipyramid with edge-briding ligands.

In contrast, the metal–metal bonding in the face-bridged octahedral clusters can be represented in terms of 12 edge-localized two-center two-electron bonds. The removal of a metal vertex with four ($1\sigma + 2\pi + 1\delta$) metal orbitals leaves four out-pointing orbitals on the square face of the cluster. These are shown in Figure 12 and generate a_1, e, and b_1 symmetry-adapted combinations. Since only the a_1 combination is sufficiently bonding to be occupied by an electron pair, the overall effect of removing the metal vertex is a loss of three metal–metal bonding molecular orbitals. The loss of a second trans vertex similarly leads to a decrease of three metal–metal bonding orbitals.

Summary

This paper has demonstrated the close relationship in the electronic structures of clusters with π-donor and π-acceptor ligands. Both classes of ligands enhance the strengths of the metal–metal bonds by limiting the extent of electron density in metal–metal antibonding molecular orbitals. The large d band-

(20) Bertrand, J. A.; Cotton, F. A.; Dollase, W. A. *Inorg. Chem.* **1963**, *2*, 1166.

Table III. Extended Hückel Parameters[a]

		H_{ii}, eV	ζ_1[b]	ζ_2[b]	C_1[c]	C_2[c]
Mo	4d	-10.50	4.540	1.900	0.5899	0.5899
	5s	-8.34	1.960			
	5p	-5.24	1.900			
Cl	3s	-26.30	2.033			
	3p	-14.20	2.033			
C	2s	-21.40	1.625			
	2p	-11.40	1.625			
O	2s	-32.30	2.275			
	2p	-14.80	2.275			
H	1s	-13.60	1.300			

[a] Hückel constant k = 1.75. [b] Slater-type orbital exponents. [c] Coefficients used in double-ζ expansion.

Table IV. Bond Lengths (Å)

Mo-Mo	2.61	Mo-C	2.06
Mo-H	1.70	C-O	1.20
Mo-Cl	2.48		

widths for the earlier transition metals lead to additional inaccessible molecular orbitals derived from the d^δ band. The number of these inaccessible orbitals depends crucially on the relative disposition of the metal and bridging ligand polyhedra. When the ligands are located on the faces, the resultant spectrum of metal-metal bonding orbitals leads to a cluster valence electron counter of 84 (e.g. $[Mo_6Cl_{14}]^{2-}$). Related nido and arachno clusters have 68 and 52 valence electrons, respectively. When the ligands are located on the edges, the preferred electron count is 76 (e.g. $[Nb_6Cl_{18}]^{4-}$) and the related nido and arachno clusters have 66 and 56 valence electrons, respectively.

For both classes of clusters the removal of an M-Cl fragment leads to a decrease of five in the total number of metal-chlorine bonding molecular orbitals. In the face-bridged clusters the loss of the M-Cl fragment also destabilizes three of the bonding skeletal MO's, and consequently the total electron count drops by 16 for the loss of each metal atom. In contrast, the loss of an M-Cl fragment from the edge-bridged clusters does not affect the number of bonding skeletal MO's and the electron count is reduced by only 10. These differences have been interpreted in terms of both delocalized and localized bonding models.

Acknowledgment. The SERC is thanked for financial support.

Appendix

The extended Hückel method[21] was used in all calculations. Values of the parameters are given in Table III. Bond lengths are listed in Table IV.

Registry No. $[Mo_6Cl_{14}]^{2-}$, 51364-21-7; $[Mo_5Cl_{13}]^-$, 99727-63-6; $[Mo_4Cl_{12}]$ (square planar), 101349-43-3; $[Mo_6Cl_{18}]^{2+}$, 101375-16-0; $[Mo_5Cl_{17}]^{3-}$, 101349-44-4; $[Mo_4Cl_{16}]^{8-}$, 101349-45-5; $[Mo_4Cl_{12}]$ (butterfly), 101349-46-6.

(21) Hoffmann, R. *J. Chem. Phys.* **1963**, *39*, 1397.

Contribution from the Department of Chemistry, University of Canterbury, Christchurch, New Zealand

Chloro Complexes of Cobalt(III) and Chromium(III) with 2,2-Dimethyl-1,3-diaminopropane. Synthesis, Characterization, and Acid Hydrolysis Kinetics

Donald A. House

Received September 19, 1985

trans-$CoCl_2(Me_2tn)_2^+$ (ClO_4^- and $ZnCl_4^{2-}$ salts) and *mer*-$[CoCl(Me_2tn)(tri)]ZnCl_4$ (tri = $NH_2CH_2C(CH_3)_2CH_2N{=}CHC(CH_3)_2CH_2NH_2$) have been isolated (after HCl workup) from the dioxygen oxidation of $CoCl_2{\cdot}6H_2O$ and Me_2tn (1:2 mole ratio) in MeOH at room temperature. A similar reaction with an equivalent mixture of $CoCl_2{\cdot}6H_2O$, Me_2tn, and en results in the isolation of *trans*-$[CoCl_2(Me_2tn)(en)]ClO_4$. The *trans*-$CoCl_2(Me_2tn)_2^+$ cation reacts with pyridine in aqueous solution to give *trans*-$CoCl(Me_2tn)_2(py)^{2+}$, which can be isolated as the $ZnCl_4^{2-}$ salt. Reaction of Me_2tn (2 mol) with $CrCl_3{\cdot}6H_2O$ (1 mol) dehydrated in boiling DMF results in the precipitation of *trans*-$[CrCl_2(Me_2tn)_2]Cl$, and ClO_4^- and $ZnCl_4^{2-}$ salts can be obtained by metathesis. Kinetic parameters [$k_H(298)$ (s^{-1}), E_a (kJ mol^{-1}), $\Delta S^\ddagger_{298}$ (J K^{-1} mol^{-1})] for the loss of the first chloro ligand in 0.1 M HNO_3 from *trans*-$CoCl_2(Me_2tn)_2^+$, *trans*-$CoCl_2(Me_2tn)(en)^+$, *trans*-$CrCl_2(Me_2tn)_2^+$, and *mer*-$CoCl(Me_2tn)(tri)^{2+}$ are respectively 5.57×10^{-3}, 96.8 ± 2, +28 ± 4; 3.22×10^{-4}, 98.0 ± 1.2, +8.5 ± 3; 2.20×10^{-5}, 103.6 ± 1.3, +5 ± 2; and 1.30×10^{-3}, 75 ± 2, -57 ± 4.

Introduction

As part of a continuing program to investigate analogous Co(III) and Cr(III) complexes with polyamine ligands, we describe here some chloro complexes containing Me_2tn[1] bound to the central metals. This diamine, when acting as a bidentate ligand, will form a six-membered ring, and the properties of the resulting complexes can be compared with those of the unsubstituted tn systems.

The synthesis of Me_2tn,[2a] while not difficult, is time-consuming. *trans*-$CoCl_2(Me_2tn)_2^+$ was described in 1946;[2b] since that time, the ligand has become commercially available, and structural studies have now been reported for the Zn(II), Cd(II), and Hg(II) complexes.[3] The earlier work[4] on *trans*-$CoCl_2(Me_2tn)_2^+$ showed that the rate of loss of the first chloro ligand in acidic solution was considerably slower (10 times) than that from the corresponding complex containing the unsubstituted diamine (tn). This is the reverse of the situation for five-membered chelate ring complexes,[5] and the basis for this observation has never been adequately explained.[6]

We were also interested in reinvestigating the synthesis of *trans*-$CoCl_2(Me_2tn)_2^+$ as we have recently found[7-9] that chloro-

(1) Abbreviations used: en = $NH_2(CH_2)_2NH_2$, tn = $NH_2(CH_2)_3NH_2$, ibn = $NH_2C(Me)_2CH_2NH_2$, pn = $NH_2CH(CH_3)CH_2NH_2$, Me_2tn = 2,2-dimethyl-1,3-diaminopropane = dan = $NH_2CH_2C(CH_3)_2CH_2NH_2$, dien = $NH_2(CH_2)_2NH(CH_2)_2NH_2$, dpt = $NH_2(CH_2)_3NH(CH_2)_3NH_2$, py = pyridine, DMF = dimethylformamide.

(2) (a) Lambert, A.; Lowe, A. *J. Chem. Soc.* **1947**, 1517. (b) Bailar, J. C., Jr.; Work, J. B. *J. Am. Chem. Soc.* **1946**, *68*, 232.

(3) Cariati, F.; Ciani, G.; Menabue, L.; Pellacani, G. G.; Rassu, G.; Sironi, A. *Inorg. Chem.* **1983**, *22*, 1897.

(4) Pearson, R. G.; Boston, C. R.; Basolo, F. *J. Am. Chem. Soc.* **1953**, *75*, 3089.

(5) Alexander, M. D. *Inorg. Chem.* **1966**, *5*, 2084.

(6) Basolo, F.; Pearson, R. G. *Mechanisms of Inorganic Reactions*; Wiley: New York, 1958; p 120.

0020-1669/86/1325-1671$01.50/0